Scientific Contributions Oil & Gas, Vol. 49. No. 2, June: 1 - 24

SCIENTIFIC CONTRIBUTIONS OIL AND GAS

Testing Center for Oil and Gas
LEMIGAS

Journal Homepage:http://journal.lemigas.esdm.go.id
ISSN: 2089-3361, e-ISSN: 2541-0520

Petrophysical Evaluation of Lam Member Reservoir, Madbi Formation (Late Jurassic), using Well Log and Core Data in Habban Field, Sab'atayn Basin, Yemen

Ali S. Ghurab[1], Ahmed N. Al-Dujaili[2], Adel M. Al-Matary[1], Basim S. Al-Khirbash[1], Mohammed. M. H. Hakimi[3], and Azmi, S. Al-Audi[1]

[1]Sana'a University, Faculty of Petroleum and Natural Resources
Petroleum Engineering Department Sana'a, Yemen.

[2]Amirkabir University of Technology/ Petroleum Engineering Department
No. 350, Hafez Ave, Valiasr Square, Tehran, Iran 1591634311.

[3]Geology Department, Faculty of Applied Science
Taiz University, 6803 Taiz, Yemen.

Corresponding Author : Ahmed N. Al-Dujaili (ahmed.noori203@aut.ac.ir)

Manuscript received: January 13th, 2025; Revised: January 26th, 2026
Approved: January 27th, 2026; Available online: June 3th, 2026; Published: June 3th, 2026.

ABSTRACT - The present work aims to quantify the Lam lithological and reservoir petrophysical characteristics of the Late Jurassic in the Habban oil field, Marib Shabwah Basin, Yemen, from the wireline logs and core data. The results revealed that the Lam Member rocks consist of an interbedded sequence of claystone, intercalated limestone, dolomite claystone, and sandstone. Lam Member lithology consists of clayey and strongly carbonate-cemented, very fine to coarse-grained Sandstone, divided into three main layers with possible reservoir units in the upper and lower sections. The Lam Member rocks are encountered with a relatively thick thickness reaching up to 5008 m and have reasonable porosity (11-25%), shale content (15-25 %), and high hydrocarbon saturation in the Habban oil field up to (70%) with maximum pay thicknesses reaching 40 m. A scatter plot of petrophysical gamma ray values versus core gamma ray values gave an approximate linear relationship. Also, Cross-plots of porosity-density values versus core values revealed a linear relationship between the two datasets. Poor-sorting, pore-filling with clay, and carbonate cementation are the main causes of poor reservoir quality. The Lam reservoir is a tight or unconventional that will rely on Perforating, natural fracturing, and/or fracture stimulation to produce oil.

Keywords: petrophysics, reservoir properties, lam member, habban field, sabatayn basin.

How to cite this article:

Ali S. Ghurab, Ahmed N. Al-Dujaili, Adel M. Al-Matary, Basim S. Al-Khirbash, Mohammed. M. H. Hakimi, and Azmi S. Al-Audi 2026, Petrophysical Evaluation of Lam Member Reservoir, Madbi Formation (Late Jurassic), using Well Log and Core Data in Habban Field, Sab'atayn Basin, Yemen, Scientific Contributions Oil and Gas, 49 (2) pp. 1 - 24. DOI org/10.29017/scog.v49i2.2005.

INTRODUCTION

The appraisal of petrophysical properties is a vital parameter for comprehending the reservoir's attitude and optimizing hydrocarbon recovery (Oktaviany et al., 2022; Wardhana et al., 2022) Uzbekgaliev et al., 2025). Petrophysical properties (including porosity, permeability, fluid saturation, and lithology) supply major insights into how hydrocarbons are distributed in the formation, transmitted, and produced to ease decisions of exploration, drilling, and production strategies (Casto et al., 2001; Abilkhasimov et al., 2025; Kashman et al., 2025).

Almost 50 years ago, the evaluation of subsurface formations related to drilling oil wells became an inclusive process, encompassing all techniques for coring, logging, testing, and sampling (Al-Dujaili 2024; Ronlei et al., 2025). The uncertainty associated with petrophysical properties will negatively influence decision-making in the process of economic investment in the reservoir (Al-Dujaili 2023; Ragil et al., 2024).

Yemen is located on the southwestern margin of the Arabian Plate (Al-Matary 2007). Mesozoic breakup of the Gondwanaland super-continent was associated with major rifting in the late Jurassic and early Cretaceous (Redfern & Jones 1995). The concerned field straddles the northern branch of the Sab'atayn Basin, which is a NW-SE trending late Jurassic intra-cratonic rift basin that lies in southwestern Yemen (Albaroot et al., 2024).

The NW-SE trend of the Yemeni Mesozoic rifts reflects an inheritance from deep-seated Pre-Cambrian structural trends observed throughout the Arabian Plate, known as the Najd trend (Beydoun 1991; El-Ata et al., 2013). It is part of an extensive system of basins that trend across southern Arabia and the Horn of Africa, from Sana'a in the northwest to the east coast of Somalia in the south (Mabon & Mason 2022). The Sab'atayn Basin is located between the Jahi-Mukalla High in the East and the Mahfid High in the West (Sachsenhofer et al., 2012). In the South, the Jabal al Aswad Uplift separates the Sab'atayn Basin from the Cretaceous Balhaf Graben (Al-Matary et al., 2018; Abudeif et al., 2024). Habban Field produces oil from the igneous and metamorphic Proterozoic Basement and from the overlaying sedimentary rocks the Jurassic Kuhlan and Shuqra Formations (Hakimi et al., 2022). The Lam Member is also considered a secondary target in the Field (Sellar et al., 2014).

This study analyzes the petrophysical characteristics of the Lam Reservoir using well logs and core data to estimate reservoir properties, compares well log and core data parameters using a cross-plot, and provides quantitative and qualitative interpretations of the Lam Reservoir in the Habban field. This data will create a clearer view of which intervals are likely to flow oil and match with some well tests. The development plans/production profiles provided should be based on current knowledge of the Lam reservoir.

Data collection and appraisal activities should continue and will lead to a better understanding of reservoir performance. Additional performance data is necessary to calibrate reservoir characteristics. As more data becomes available, development plans and drilling programs are subject to change based on emerging field information, so novelty of this study lies in updating the lithological and petrophysical evaluation of the Lam reservoir, which was previously studied with a gap in accuracy and limited data available, as a results to the new advanced data from the well drilling process, core analysis, and wireline logs in the Habban field.

Geological setting

Habban Field, Block S2, (Al Uqlah) is located in the province of Shabwah in central Yemen and lies along the northern border of the Shabwah province, south and west of the Hadramawt province (Abudeif et al., 2024). The capital of Shabwah governorate, the city of Ataq lies approximately 90 km SSW from Block S2. The entire surface area of Block S2 consists of flat sandy desert with some dune ridges in the western and northern parts of the block (Hadden 2012; Hatem et al., 2016).

The overall altitude of the block is around 800 masl with the proposed development area of 904 km^2. The eastern part of the block, represents outliers from the Hadramawt Plateau with no topographic features except the high area of the Jabal Al Uqlah and the most prominent and block-naming landmark in Armah District in Block S2 (Edgell 2006).

The Habban Field is divided into two productive areas: North and Central. These horse blocks, separated by a deep half graben, were created during late Jurassic rifting (Figure 1) (Ghiglione & Abbasi 2012). A total of 4357 km of 2D seismic lines of four vintages as well as 387 km^2 of 3D seismic data (Bawazer et al., 2018).

The proposed development area is located in the central part of Block S2 and comprises geological the “Central Basement High” and the “Al Nisr High” with the adjacent Half Graben areas. The NW-trending Sab’atayn Basin (also called Marib-Shabwa-Al Jawf Basin) is a Mesozoic rift basin in the Arabian Peninsula that follows a deep-seated Proterozoic structural trend (Redfern and Jones, 1995; Watchorn et al., 1998) (Figure 2).

Basin formation resulted from an extensional phase related to the separation of India from Africa -Arabia (Redfern & Jones 1995; Ziegler 2001) (Figure 3). The stratigraphic subdivision of the basin fill according to Beydoun et al. (1998) is displayed in (Figure 4).

Pre-rift deposits for the Kuhlan Formation are represented by non-marine to shallow-marine clastic rocks (Beydoun et al., 1996) overlain by shallow-marine carbonates (Shuqra Formation). A latest Triassic to Middle Jurassic age is generally accepted for both formations (Al-Wosabi & Wasel 2011). Stephenson and Al-Mashaikie (2011) provide evidence for a Late Carboniferous age for

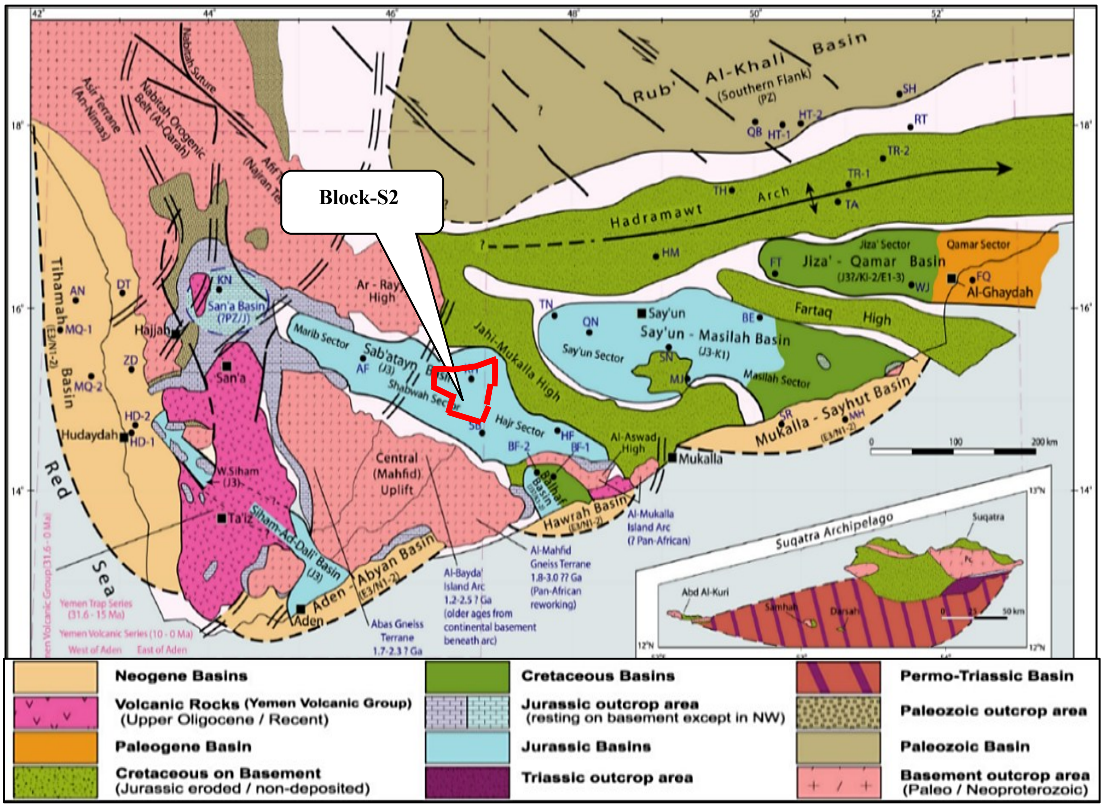

Figure 1. Sedimentary Basins of Yemen showed Block S2 Location.

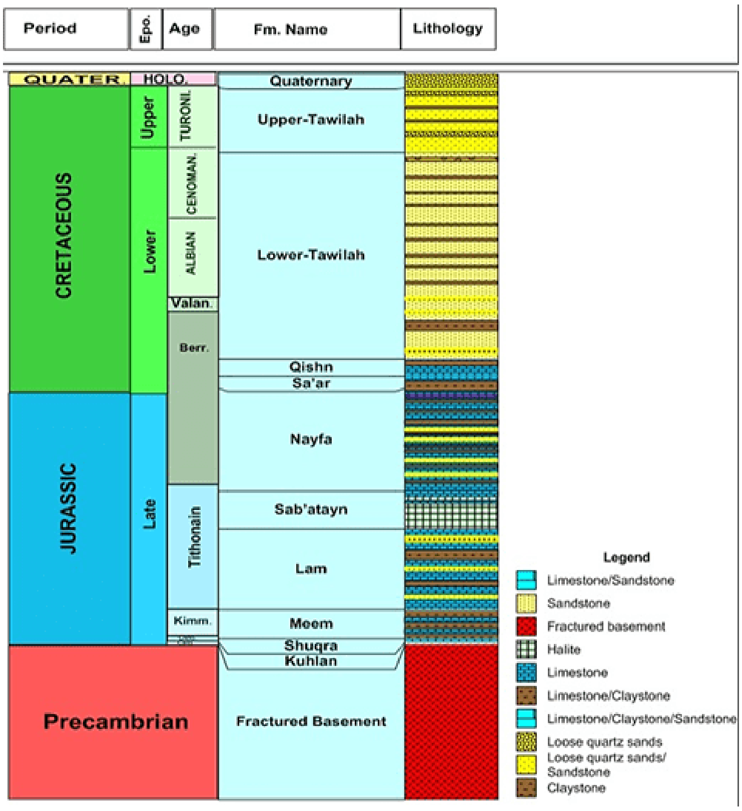

Figure 2. Stratigraphic column of Sabatayn basin, with the stars pointing at reservoir targets relevant to Habban Field Block S2. (Modify after Beydoun, et al., 1998; As-Saruri, et. al 2013).

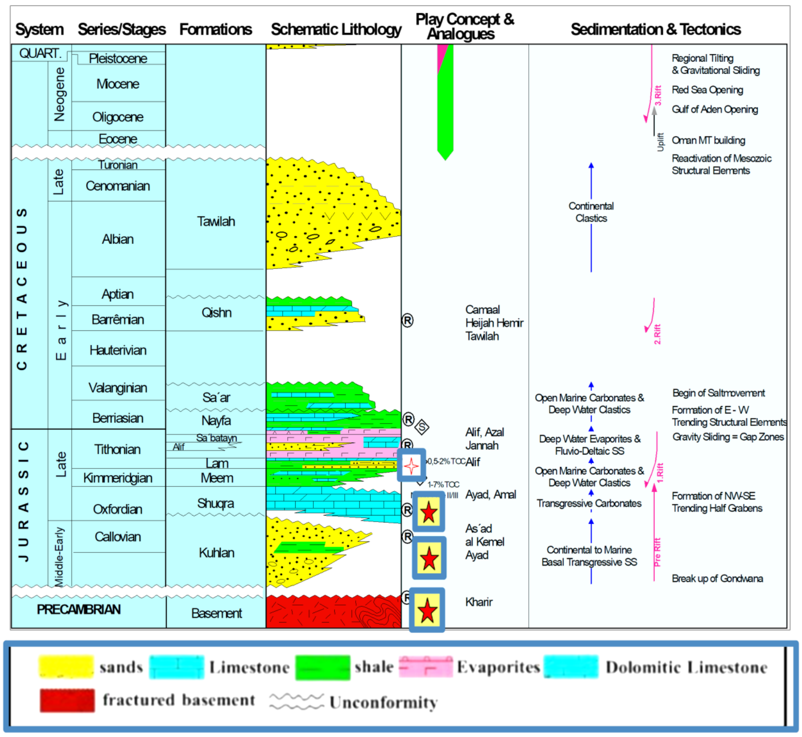

- **Source:**
Lam and Meem (Madbi formations)

- **Reservoir:**
Primary: Basement, Kohlan and Shuqra Formations.
Secondary: Lam member

- **Seal:**
Shales of the Meem Member (L. Madbi. Fm)
Shuqra. Fm

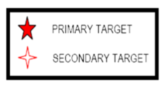

Figure 3. Lithostratigraphic and chronostratigraphic chart of Sab'atayn Basin (Modify after Beydoun, et al., 1998; As-Saruri, et. al 2013).

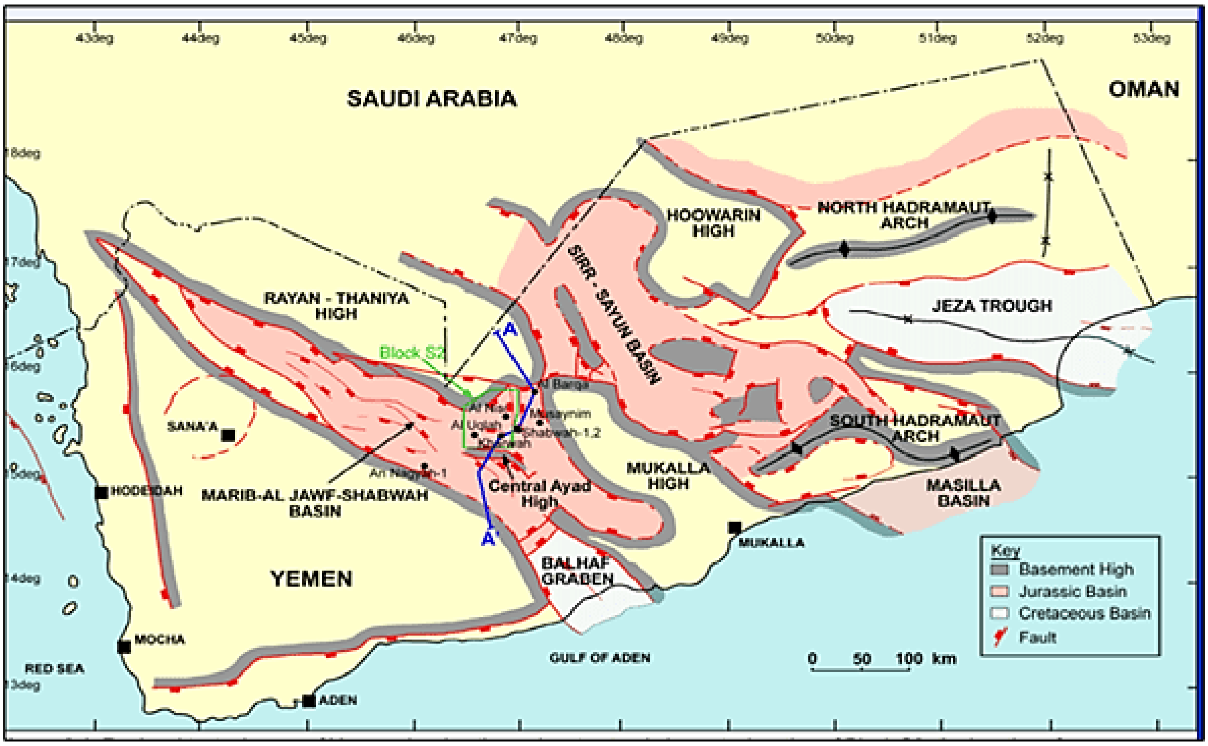

Figure 4. Regional tectonic map of Yemen showing the major structure elements with location of Block S2 (Redfern & Jones 1995).

the lower part of the Kuhlan Formation. Late Jurassic (Kimmeridgian–Tithonian) rifting resulted in the deposition of the Madbi Formation exceeding 1,500 m in thickness (Seaborne 1996; Worden 2006). It comprises muddy limestones and chalks with shale horizons. An occasional rich, but low-diversity Nannofossil/Dino cyst assemblage supports a relatively deep, partly restricted environment (Brannan et al., 1999). Beydoun et al. (1998) subdivide the Madbi Formation into a lower Meem Member and an upper Lam Member. Simultaneously continental sediments filled the grabens along rift margins (Ahlbrandt 2002; Adams 2011). During the late stages of the syn-rift phase, ocean circulation in the Sab'atayn Basin became restricted, and an evaporation succession (Sab'atayn Formation) with an estimated original thickness of about 300 m was deposited (Seaborne 1996; Al-Areeq et al., 2018 and 2019). Massive halite occurs in the basin center, whereas anhydrite and clastic rocks prevail along the basin margins Interbedded thin shale are rich in organic matter (Brannan et al., 1999). The present thickness of the Sab'atayn Formation is strongly controlled by salt tectonics. The Sab'atayn Basin Rifting was initiated in the Late Jurassic and was followed by thermally driven (post-rift) subsidence and a period of uplift and erosion during the Early Cretaceous. The most likely basement of Sab'atayn Basin is the NESW trending Abbas's gneiss terrane, which outcrops to the NE and SW of the basin (Albaroot et al., 2016).

Rift shoulder uplift during the Tertiary was associated with extension in the Gulf of Aden and Red Sea areas leading to the development of the present erosion levels. The Sab'atayn Basin is an NW-SE trending rift basin comprising an asymmetric half-graben, inherited from the Najd Trend. A large intra-basinal high was active and controlled sedimentation during the Late Jurassic and Cretaceous (Bosence 1997).

Two major periods of extension have been identified in the Sab'atayn Basin (Elhossainy et al., 2022), namely the Kimmeridgian - Tithonian (Late Jurassic) first rift and Sag Phase and the Hauterivian-Barremian (Early Cretaceous) second rift phase (Al-Matary 2003). During the Middle to Late Jurassic, the area was a tectonically quiescent platform; a gradual marine transgression took place with slight deepening of marine conditions (Ellis et al., 1996).

METHODOLOGY

The study is based on data from four wells (H-17, NIL-1, H-28, and JAM-1) Figure,5 which penetrated the Lam reservoir Late Jurassic which is a secondary shallow target in the Habban Field. Lam reservoir consists of thin bed sands from a distal turbidity system with restricted sand continuity and with marginal porosity and permeability values due to carbonate cementation. Data include well logs for 4 wells and cores analysis from two wells H-28 and JAM-1. Well logs including gamma ray, density, neutron, sonic, resistivity (shallow and deep), and photoelectric factor (PEF) logs were interpreted to assess the hydrocarbon potentiality of Lam reservoir. A complete set of wire line log data for study wells and drilling reports was acquired from the internal reports of the Petroleum Exploration and Production Authority-Yemen (PEPA). Tech Log and Petrel Schlumberger softwares were used to conduct the qualitative and quantitative analyses using LAS files given in Table 1. The intrusion of the Sab'atayn salt is well seen in the western side of inline section 1235 associated with basement reservoir uplift (Figure 6).

Table 1. Wire line logs run at Lam member in the study wells

Well	Lam interval (m)	Wireline data
NIL-1	2052-2374	GR, CAL, CNC, ZDEN, ZCOR, PE, DT, RMLL, RS, RD
JAM-1	2316-3096	GR, HEXADIP, DLL, MLL, DAL, SP, TTRM, ZDL, CN.
H-17	2083-2422	GR, TNPH, ROHB, PEB, P16H, P28H, P4OH, A28H, A40H
H-28	2000-2266	GR, RD, BHI, and Sonic

The water saturation was computed using the Indonesian equation, in which a factor and cementation exponent were derived from core analysis (a= 1, m=1.2, n=2). The logs were also used for well correlation. The identified reservoir tops in the wells were tied to the seismic sections for horizon identification and mapping with the aid of the check shot data from the wells. Cores were used as a reference and calibration to compare with the lithology and petrophysical properties interpreted from the wire line logs (Figure 7). Additional information came descriptions were carried out on the available cores, recording lithology, sedimentary structures, diagenetic features, visible porosity and fracture porosity. These data will be plotted , correlate and processes to calculate the petrophysical properties of Lam reservoir. Analysis of both cores and logs enable the main stratigraphic sequences and the Lam Reservoir Characteristics.

RESULT AND DISCUSSION

The results and discussion obtained from this work are coined around the properties that define a reservoir as being either prolific or not. These parameters are computed, using empirical petrophysical equations.

Lithological and mineralogical

Lithological and mineralogical components of Lam Member was identified using different cross plots where different types of matrices were

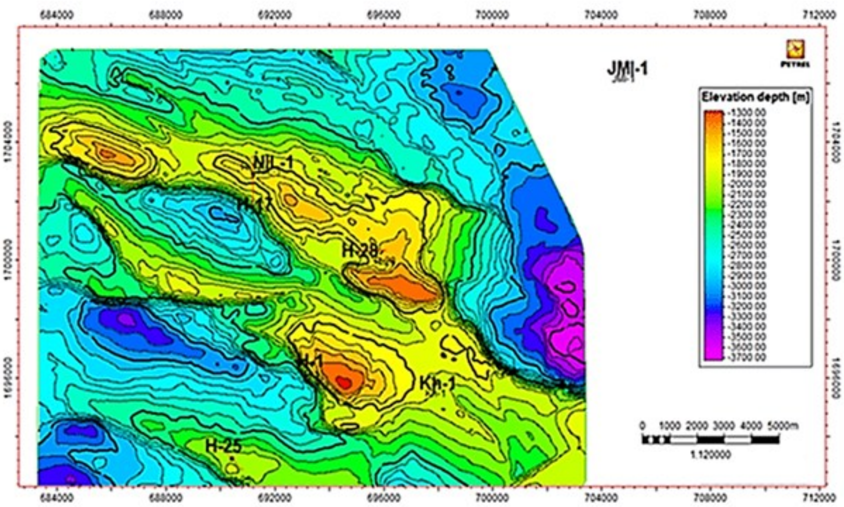

Figure 5. Lam Depth Map with Location of the study area wells in Block S2

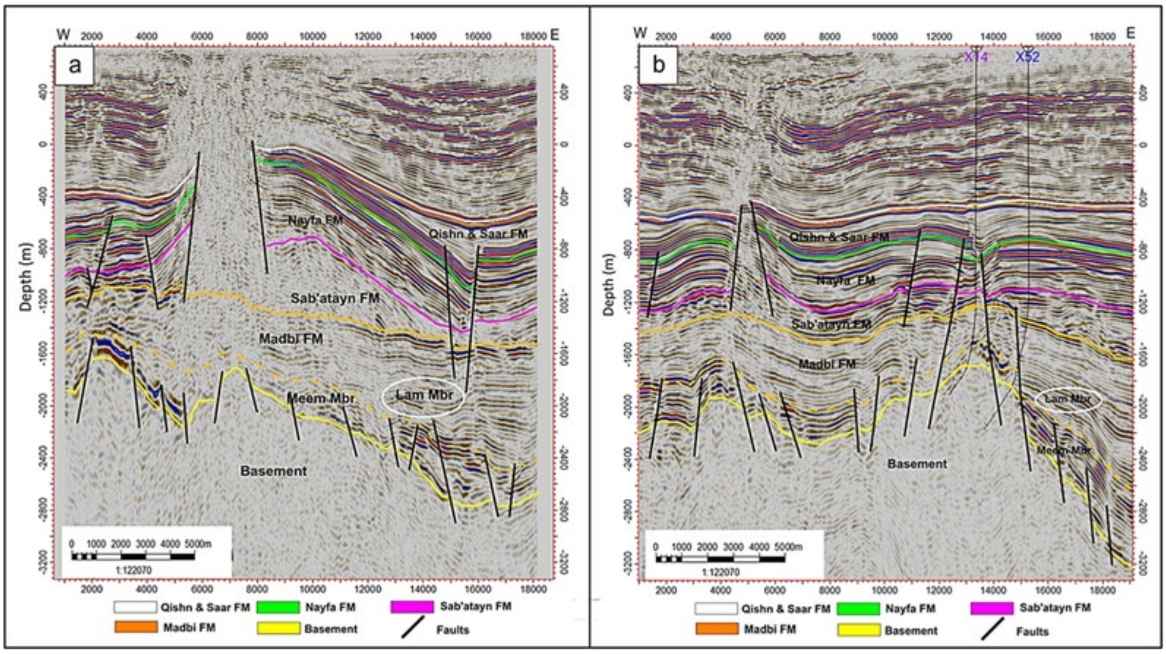

Figure 6. 2D interpreted inline seismic section, a) 1235 and b) 1345 (After Bawazer et al., 2018).

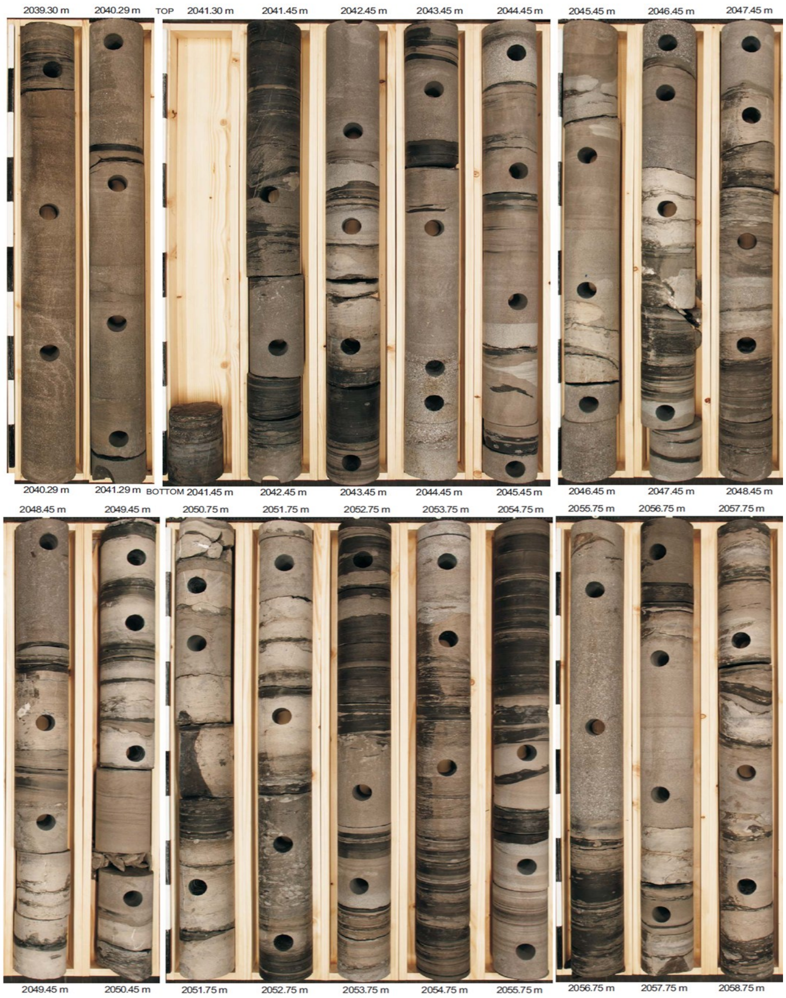

Figure 7. Large-Scale Cores for HABBAN 28.

observed by integrating different well logs. Lithology consists of carbonate interbedded with sequence of claystone with intercalated sandstone very fine to coarse-grained contains Clayey to strongly cemented of Calcite. From the Core samples analyses from H-28, interval (2039.30 to 2060.15 m) in Lam member, the samples can be classified as silty to sandy mudstones to wackestones. Fecal pellets occur in high abundances in some samples indicating pervasive bioturbation (Figures 8 and 9).

Foraminifera tests and tiny shell debris occur subordinately. Bio clasts consisting of phosphate occur in traces. Pyrite is common, it occurs mainly as tiny dots within the groundmass and partly as infill of Bio clasts. All studied samples are strongly bioturbated. The micritic groundmass indicates deposition under low energy conditions. low amounts of Bio clasts and the occurrence of pyrite point to a stressed setting. Macroscopic identifiable trace fossils (except Glossifungites ichnofacies) also indicate a stressed setting. The limestones are interpreted to have been deposited in a quiet, somehow restricted depositional setting (basinal plain).

The average mineralogical composition derived by XRD-analysis is quartz, traces of potassium feldspar, plagioclase calcite, traces of ankerite, traces of pyrite and clay minerals mica. Clay mineralogy consists of illite, kaolinite, chlorite and mixed layer minerals showed in figure 6 below

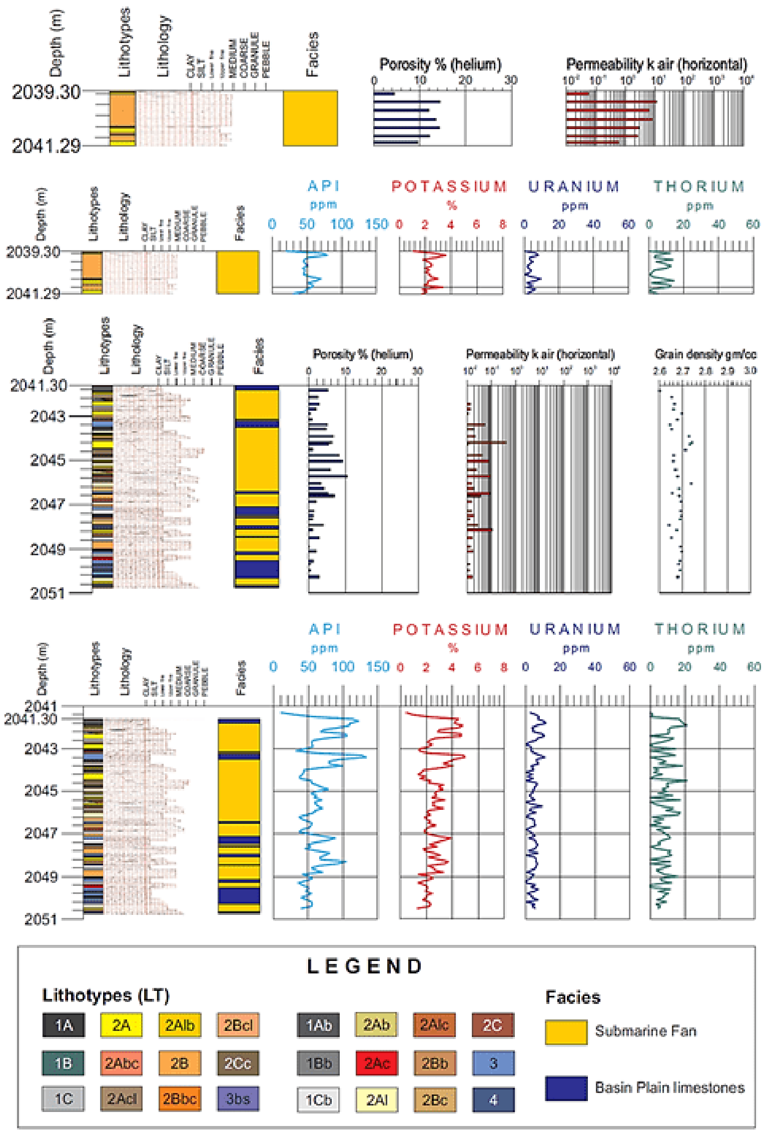

Figure 8. Porosity, Permeability, Density Log, and Spectral Core Gamma Log for the sections (2039.3-2041.29) and (2041.3-2053) for the well H-38, with identifying lithology.

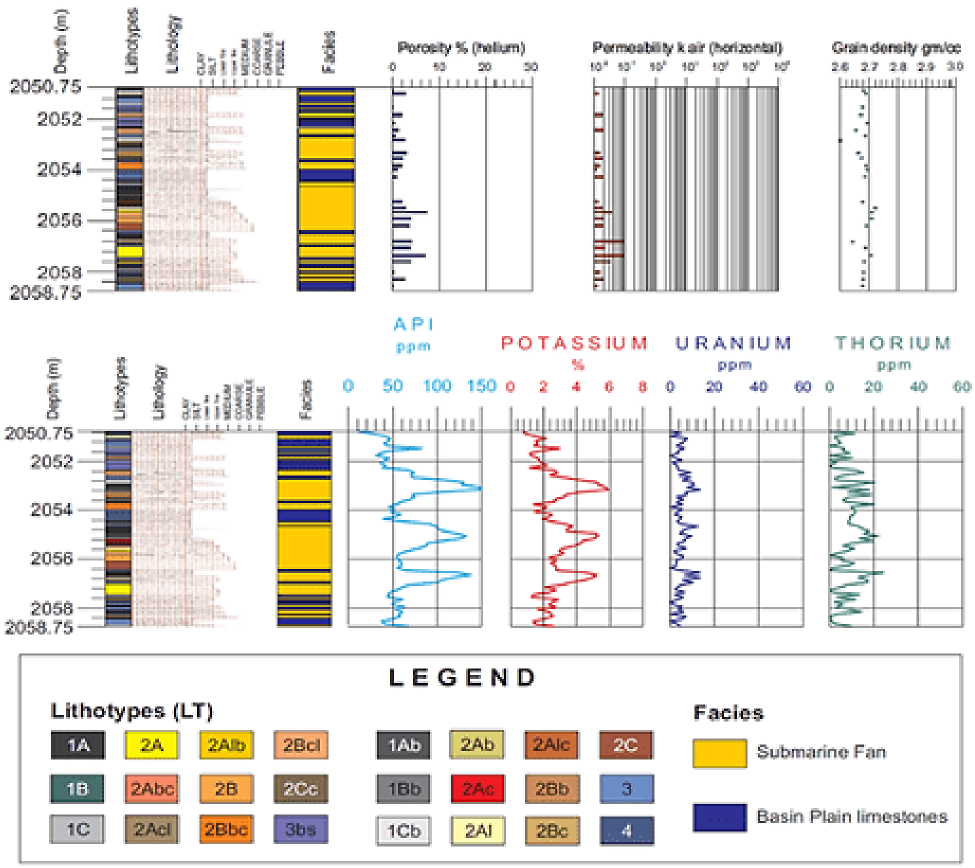

Figure 9. Porosity, Permeability, Density Log, and Spectral Core Gamma Log for the section (2050.75-2058.75) for the well H-38, with identifying lithology.

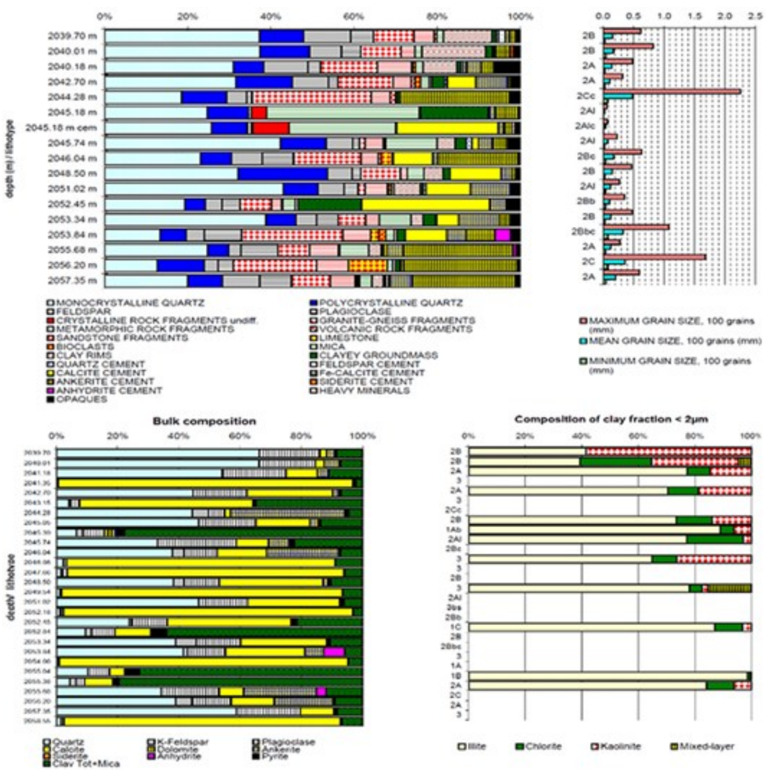

Figure 10. Results of thin- section analyses (XRD) of H-28 core sample.

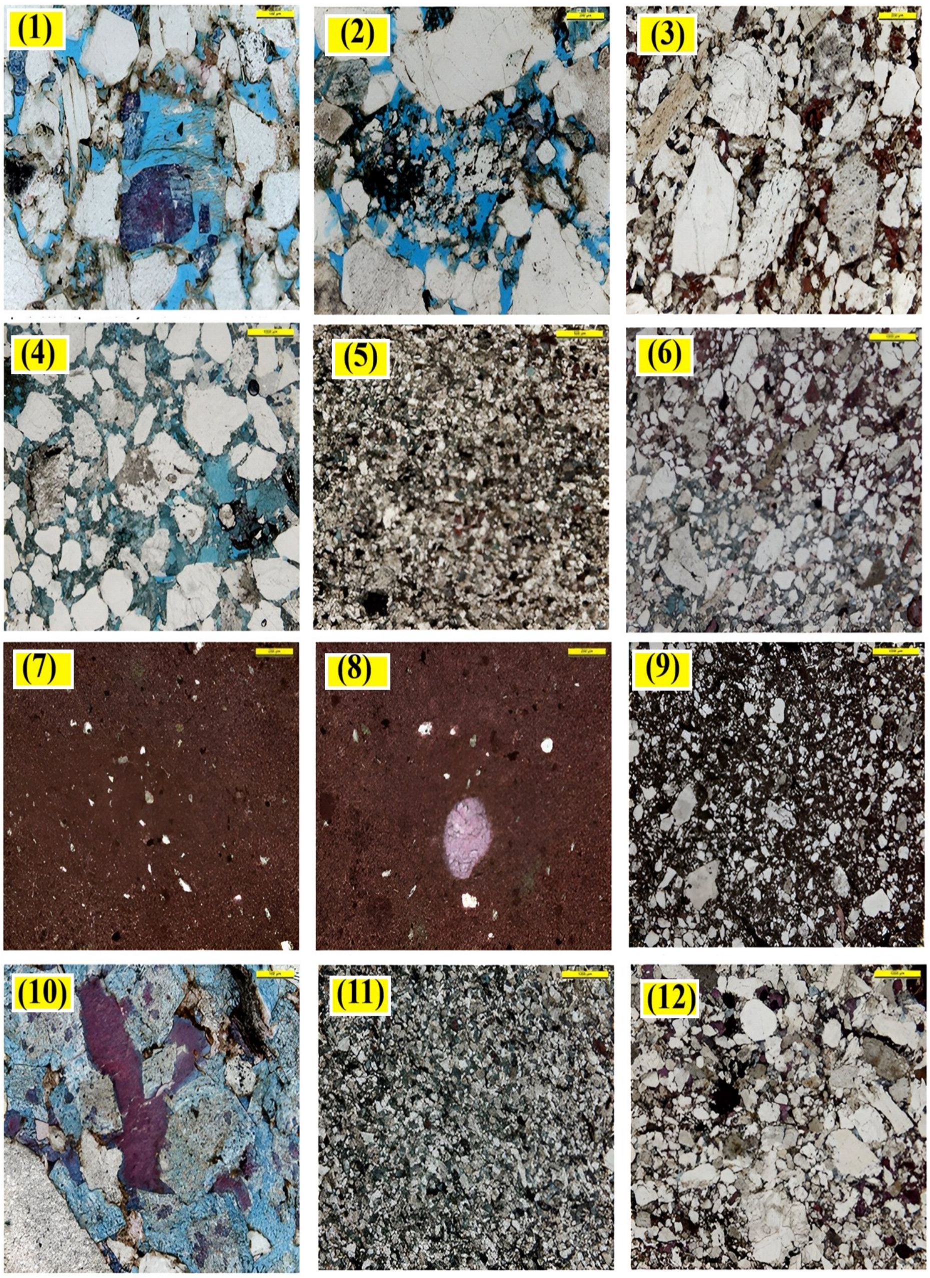

Figure 11. Thin-section and Sem-Microphotographs of H-28 from depth 2039.7 to 2058.55 m

with XRD analysis. Well H-28 has core in Lam Member and because of no wire line information within the Lam interval analyzed, except sonic (DT), Gamma Ray (GR) and Deep Resistivity (RD) (Figures 10 and 11).

The subsurface lithologies were identified first using a gamma ray log indicating a low signature for sand and a high for shale. Through lithology identification, reservoir sands were marked throughout the wells. After identifying the sands, resistivity logs were used to indicate the fluid type in a reservoir. Petrophysical parameters such as porosity (ϕ), permeability (k), Volume of shale (Vsh), Water saturation (Sw), Hydrocarbon saturation (Sh)… etc. were calculated and the results presented in the form of graphs and tables. Table 2 illustrates the characterisitics of the core samples in Figure 9.

According to Figure 11 and Table 2, the relatively best reservoir properties are present in fine-medium to medium-grained sandstones of lithotype 2B (mean permeability 2.60 md, mean

Table 2. Characterisitics and overview of the core samples in Figure 9.

No	Characteristics	Overview
1- LT: 2B	Depth: 2039.70 m Por: 14.45% Perm: 11.08 md	Overview of fine-medium- to medium-grained, moderately sorted porous arkosic sandstone. Framework grains comprise mainly quartz, crystalline rock fragments, feldspar and plagioclase. Pore space is stained bluish.
2- LT: 2B	Depth: 2040.01 m, Por: 12.03% Perm: 6.46 md	Close-up of secondary pore space created by dissolution of unstable framework grain.
3-LT: 2A	Depth: 2042.70 m, Por: 1.97% Perm: 0.01 md	Close-up of framework grains. Note metamorphic rock fragment (center) and potassium feldspar.
4- LT: 2Cc	Depth: 2044.28 m Por: 5.36% Perm: 0.01 md	Overview of medium-coarse to coarse-grained, well sorted, strongly ankerite cemented arkosic sandstone. Ankerite cement is stained in a strong bluish color.
5- LT: 2Al	Depth: 2045.74 m, Por: 10.52% Perm: 0.09 md	Overview of very fine-grained, well sorted, moderately carbonate-cemented feldspathic litharenite. Framework grains comprise mainly quartz, mica, potassium feldspar, plagioclase and crystalline rock fragments.
6- LT: 2Bc	Depth: 2046.04 m Por: 3.45% Perm: 0.02 md	Overview of fine-medium- to medium-grained, well to moderately sorted, strongly carbonatecemented arkosic sandstone. Note different cementation: the upper part is calcite-cemented (stained reddish) whereas the lower part is ankerite-cemented (stained bluish).
7- LT: 3	Depth: 2047.66 m Por: 1.13% Perm: 0.01 md	Overview of silty to sandy mud- to wackestone. Note pyrite and lack of bioclasts.
8- LT: 3bs	Depth: 2052.18 m Por: 0.49% Perm: 0.01 md	Picture of silty-sandy mud- to wackestone. Note recrystallized bioclast in center of image.
9- LT: 2Bb	Depth: 2052.45 m Por: 1.30% Perm: 0.02 md	Picture of fine- to fine-medium-grained, strongly calcite-cemented feldspathic greywacke. Framework grains consist mainly of quartz, crystalline rock fragments, potassium feldspar, plagioclase and mica. Calcite is stained reddish.
10- LT: 2C	Depth: 2056.20 m Por: 3.52% Perm: 0.02 md	Detail of ankerite and calcite cement. The latter one postdates precipitation of ankerite cement.
11- LT: 2A	Depth: 2055.68 m Por: 7.27% Perm: 0.04 md	Overview of fine-grained, well sorted, ankerite-cemented lithic arkose. Framework grains consist mainly of quartz, crystalline rock fragments, plagioclase, potassium feldspar and mica.
12- LT: 2Bbbc	Depth: 2053.84 m Por: 2.10% Perm: 0.02 md	Overview of medium-coarse-grained, poorly to very poorly sorted, carbonate-cemented arkosic sandstone. Framework grains consist mainly of crystalline rock fragments, quartz, plagioclase, potassium feldspar, detrital limestone, bioclasts and mica. Calcite is stained reddish.

porosity 7.21%). Porosity is mainly provided by interparticle pores and secondary pore space created by dissolution of unstable framework grains. All other lithotypes exhibit lower mean permeability and porosity values. The overall poor reservoir properties are poor sorting of sandstones, resulting in high pore-space-to-pore-throat ratios, occluding clayey groundmass, and extensive carbonate cementation.

Some coarser-grained sandstone intervals are characterized by high amounts of carbonate cement, which precipitated within interparticle pore space. This indicates early cementation before compaction of sandstones. One open fracture showing a heavy oil (tar) stain is present within a limestone interval.

The cored deposits are represented by three main lithologies: very fine- to coarse-grained, slightly to strongly calcite-cemented shaly sandstones, dark grey to almost black shales, and calcareous shales and light grayish limestones (mudstones). Frequent occurrence of graded bedding, frequent occurrence of carbonaceous plant material and pyrite nodules, healed fractures and joints, two open fractures exhibiting a tar-film on the fracture plane, and carbonate concretions.

Based on the qualitative and quantitative interpretations, two reservoirs of sand in Upper and Lower Lam Reservoir were identified throughout 4 wells. The depth (m) interval of Lam Reservoir and the thickness of the reservoir in the study wells are shown in Table 3.

Table 3. Lam reservoir interval (m) and thickness in the study wells.

Well No.	Lam interval (m)	Lam thickness (m)
H-17	2075.5-2447	371.5
H-28	2000-2172.3	172.3
NIL-1	2052-2374	322
JAM-1	2316-3096	780

The heavy mineral assemblage indicates a mixed magmatic and metamorphic source area. The predominance of garnet might indicate a stronger influence of the metamorphic source area (Table 4 and Figure 12).

Table 4: Heavy minerals composition percentage for the well H-28 from core analysis

Depth	2039.7	2042.7	2045.05	2048.5	2051.02	2056.2
lithotype	2B	2A	2B	2B	2AI	2C
Zircon	28	9	32	14	3	22
Rutile	7	5	20	12	6	10
Brookite	6	1	2	0	0	1
Titanite	4	2	3	1	1	2
Monazite	2	1	2	1	0	4
Tourmaline	35	37	19	24	38	5
Garnet	17	44	21	47	52	56
Chromite	0	0	0	1	0	0
Pyroxene	1	0	1	0	0	0
Anhydrite	0	1	0	0	0	0

Neutron (NPHI) versus density (RHOB) cross plot

Cross-plot shows that the Lam Member within the indicating sandstone and carbonates are dense as compared to the shale rich clusters of data points. The presence of shale contents within the sandstone also causes the data point to cluster more towards. Limestone and dolomite line. selected wells appear to be dominantly composed of carbonates (limestone and dolomite) with sandstone which deposits and interpreted to have been formed in a submarine fan to basin plain setting. The submarine fan deposits consist of turbidity, slurry and debris flows whereas the basin plain deposits comprise limestones. NPHI vs. RHOB cross plot also indicates the presence of subordinate shale and also helps in estimating a relationship between different lithology and porosity types. Since the cross plot indicates the presence of both sandstone and carbonates which also indicates the presence of both inter granular and secondary porosity with an equal proportion. Figure 10 shows Cross Plot of Neutron Porosity (NPHI) vers Density Porosity (RHOB) which confirm Lam sequences and lithology as dominantly composed of carbonates (limestone and dolomite) with sandstone (Figure 13).

This classification is conducted based on the works carried out by different researches like (Hakimi et al. 2018). Figure 13 shows that the Lam Member is composed of carbonates and shale intercalated with sandstone. Clusters indicating

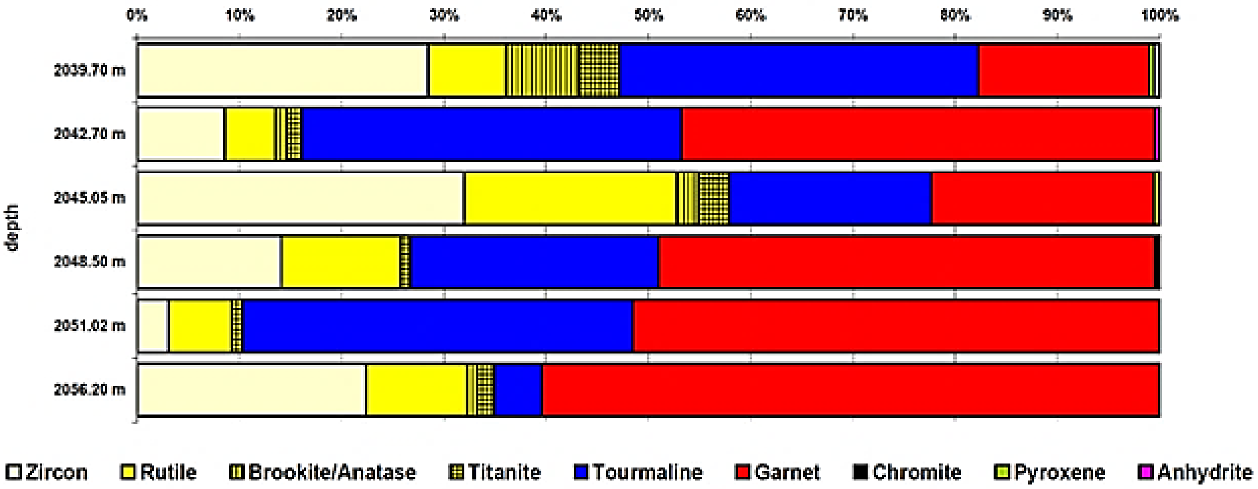

Figure 12. Heavy minerals analysis of the well H-28

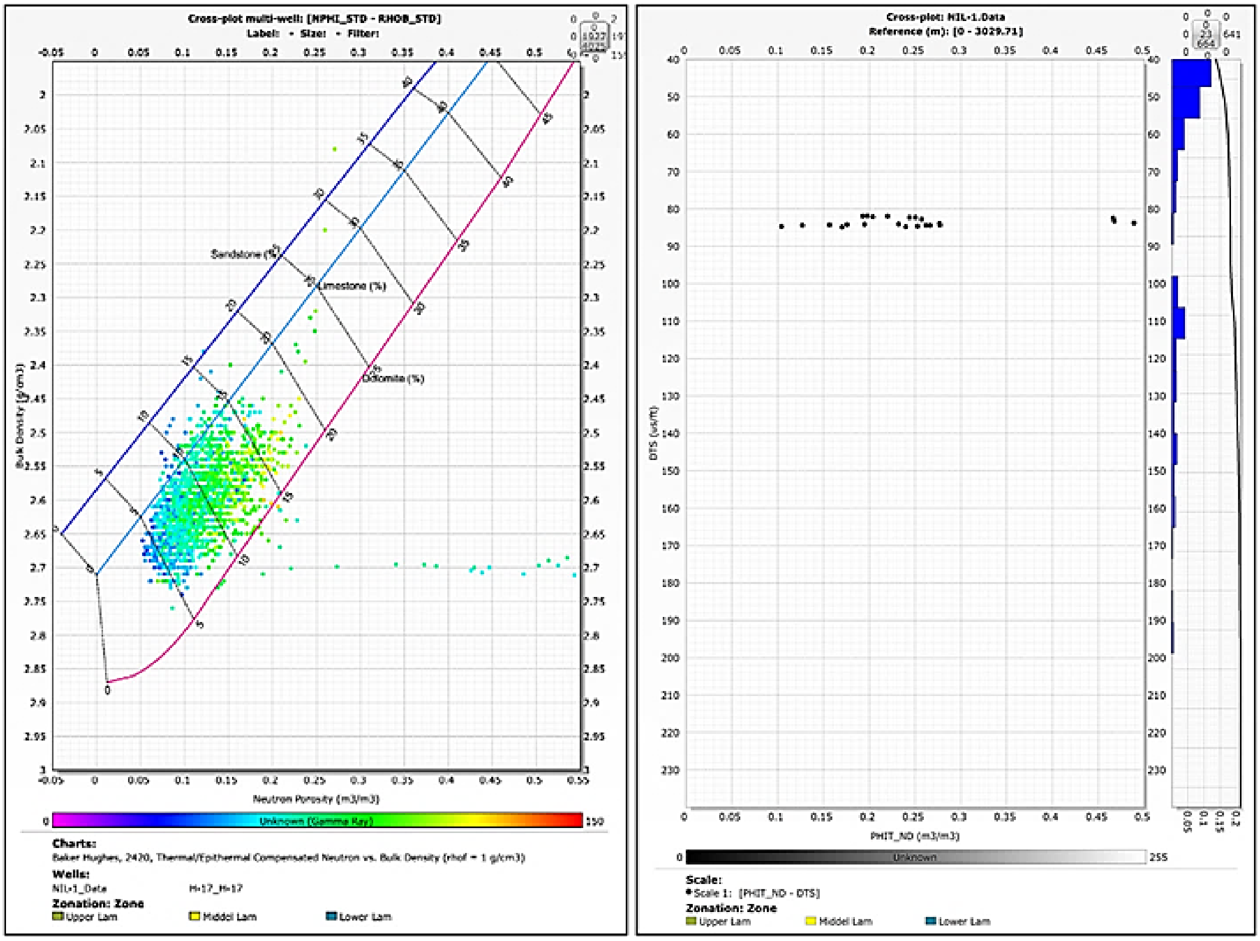

Figure 13. Left- Neutron Porosity (NPHI) vs. Density Porosity (RHOB) cross-plot for Lam Member, Right- the type of porosity within the Lam reservoir estimated by neutron-density log vs. sonic log cross plot

sandstone and carbonates are dense as compared to shale rich clusters of data points. The presence of shale contents within the sandstone also causes the data point to cluster more towards limestone and dolomite line.

Petrophysical analysis

Petrophysical properties which is essential like shale volume, total and effective porosity and fluid saturation (both oil and water) were derived by well log analysis to estimate the hydrocarbon potentiality of the Lam Member reservoir in Habban Field.

Shale volume estimation

In order to evaluate the reservoir potential, it's indispensable to calculate the shale volume content which can helps to distinguish between reservoir and non-reservoir. In addition. The results indicate that the reservoir formation shows an overall low shale volume. The V_{sh} within the reservoir of studied wells ranges from 14 to 30%. The Neutron porosity versus density porosity cross plot has been used to identify the shale habitat as shown in Figure 10. Since the presence of shale habitat affects the fluid saturation calculation therefore it is essential to apply corrections. That is why the dual water saturation model has been applied to boost up confidence for water saturation calculation.

Log derived porosity estimation

In this study total and effective porosity were estimated using Schlumberger Tech log 2018 software. The results show that the Lower Lam Member has low volume of shale, indicating that pore spaces are filled with water or oil. The total and effective porosity have been calculated by using neutron and density logs. Based on porosity classification, the Lam Member Reservoir within the studied wells show a poor to good total and effective porosity. The total and effective porosity range from 6 to 22% and 4 to 14% respectively. The type of porosity within the Lam reservoir has been estimated by neutron-density log vs. sonic log cross plot as shown in Figure 10. The reservoir formation shows the presence of both inter granular and secondary porosity. The presence of secondary pore type can be a result of partial or complete dissolution of feldspar or carbonates within the reservoir formation during various diagenetic phases and result of syn refit movement and faults which done in Jurassic, As rift topography was infilled, fine-grained clastic of the upper Lam Member spread throughout the basin. The Lam Member is the product of erosion of the emergent foot wall areas created by rifting Close to the major faults, conglomerates, sandstone and silt stone typify the Lam Member Reservoir.

Fluid saturation estimation

The fluid saturation is important to estimate the types and concentrations of fluids present in the pore spaces. The results indicate that water saturation (S_w) ranges 30–80%. Although it is important to calculate the water saturation, the more essential part is to estimate the hydrocarbon saturation and water saturation using Calculating method.

The results indicate that the Lam Member reservoir exhibits a Low to good hydrocarbon saturation (S_h) ranging 20–70%. The both types of water volume were estimated by multiplying water saturation with effective porosity. The results indicate that studied wells show low water saturation and good hydrocarbon saturation.

Net pay thickness and net/gross thickness estimation

Net pay is an important parameter to evaluate the reservoir potential as it identifies the zones having enough hydrocarbon volumes and acting as producing intervals. Net pay is a sub interval within the gross thickness and is quantified by applying petrophysical cut-offs to well log data. Net reservoir was calculated assuming <14- 30% V Shale and > 6% Porosity and S_{w} (20-80%) Cut-offs used for net pay.

Lam Member in Habban Field has a gross thickness ranging from 711 m in well (JAM-1) to 97 m in well Al Nisr-1. Lam reservoir currently has been divided in three main layers with possible reservoir units in the upper and lower sections. Lithological and petrophysical differences have been encountered for the Kharwah and Al Nilam areas (Table 5).

Table 5. Lam average net pay and porosity

Layer	Area	Avg. Net Pay (m)	Av. Porosity (%)
Upper	Al Nilam	3.85	9
	Kharwah	12.06	
Lower	Al Nilam	2.56	6
	Kharwah	3.08	4

Implication on reservoir quality

Lam reservoir is described as a turbidite deposit. Based on cuttings and well log interpretation, it has been divided in three main depositional units. Two are potential reservoir units: the upper and lower sections with a non-reservoir section in between them. The main potential reservoirs in the Lam are fluvial-delta, shallow marine, fault scarp fan turbidity sandstone and conglomerates, and locally shallow sub-tidal lime grain-stone shoals and their dolomitization equivalents. Less important potential reservoirs include fan-delta and distal turbidite sandstone.

From petrophysical point of view this reservoir has a poor quality and high heterogeneity with very thin sandstone layers surrounded by tight rocks. Reservoir quality is heavily affected by cementing events. Most important marker horizons are top Lam Member and top Meem Member (Base Lam). Lam turbidites generally represent low-quality reservoirs due to diagenetic cementation. These turbidites have been sourced from shallow shelf areas where coarse clastic fans have been deposited.

The remaining porosity is largely secondary porosity created by the breakdown and dissolution of feldspar. All the studied wells are show that there is evidence of oil in Lam Member Reservoir and was proved hydrocarbon bearing in NIL-1 by Lam interval test and in H-17 after perforating the interested reservoir zones in Lam. The main aims in this study are to evaluate the Lam reservoir. Four wells have been identified as possible potential for Lam appraisal and ranked based on the reservoir quality and STOIIP accumulation and must be considered as derived from a preliminary study.

Petrophysical evaluation from wire line logs in lam member reservoir

The main target of petrophysical analysis is to determine the hydrocarbon saturation of each reservoir across the wells, along with other petrophysical data.

In Habban-17 Several gas shows were reported in the Lam reservoir in the interval from 2085m MD to 2396m MD. At 2211m MD oil show were present in the samples with oil on the shaker; in the interval 2224-2232 the well had no return and gain return only after pumping LCM. A set of logs while tripping was recorded including GR-Resistivity and Density-Neutron. The logs show the presence of Sandstone in the interval where the shows were reported.

The porosity is ranging between 9 and 15%. At 2224 m and 2300m the presence of spike in the Density Neutron may indicate fractures. These data confirm the potentiality of the (HC) in Lam reservoir in the area. Both the oil on surface and total losses depths are associated with a low-density response from the logging while drilling tool (LWD). Without a caliper log, caving's due to bad hole can be inferred from a low-density response. The density log has a low radius of investigation compared to other logging tools and consequently it is affected by enlarged borehole. Bad hole is a good indicator of natural fractures in the Lam Reservoir. (Figure 14).

Given these positive indications it was decided to select the interval 2210 – 2215m MD to perforate Acidic and test the Lam Reservoir in H-17. A 5m interval was chosen if hydraulic fracturing was required later in the event of a no flow test from natural fractures.

This interval coincides with the depth of oil over shakers. H-17 interested intervals in the Lam Reservoir: (2096 to 2220 m), (2159 to 22171 m), (2293 to 2310) and (2363 to 2378 m). The well summary shows the distribution of “net reservoir” in H-17. It accounts for a total of 104 m TVT with an average porosity of 15 % and an average water saturation of 70% (Table 6).

Petrophysics interpretation

From the well-Log, hole size 8.5 inch, and the caliper from the Density tool show some washouts in this section (2,293 - 2,296m; 2,300 - 2,306m; 2,320 - 2,324m) up to 14". The hydrocarbon bearing zones for the Well: NIL-1 are shown in (Table 7 and Figure 15) with a cut-off for porosity 6%, water saturation 60% and shale volume 40%.

Table 6. Petrophysical parameters and summation results for the well H-17

Top MD (m)	Bottom MD (m)	Gross (m)	Net Res. (m)	Net Res. Porosity	Net Res. Perm. mD	Net Res. WS	Net Pay (m)	Net Pay Porosity	Net Pay Perm.	Net Pay WS
2096	2130	34	14	0.09	0.293	0.78	8.5	0.14	1.9	0.76
2159	2171	12	6	0.1	0.883	0.71	4	0.13	1.4	0.66
2200	2220	20	9	0.16	1.44	0.84	7	0.19	2.25	0.79
2293	2310	17	8	0.15	1.23	0.65	1	0.18	2.1	0.8

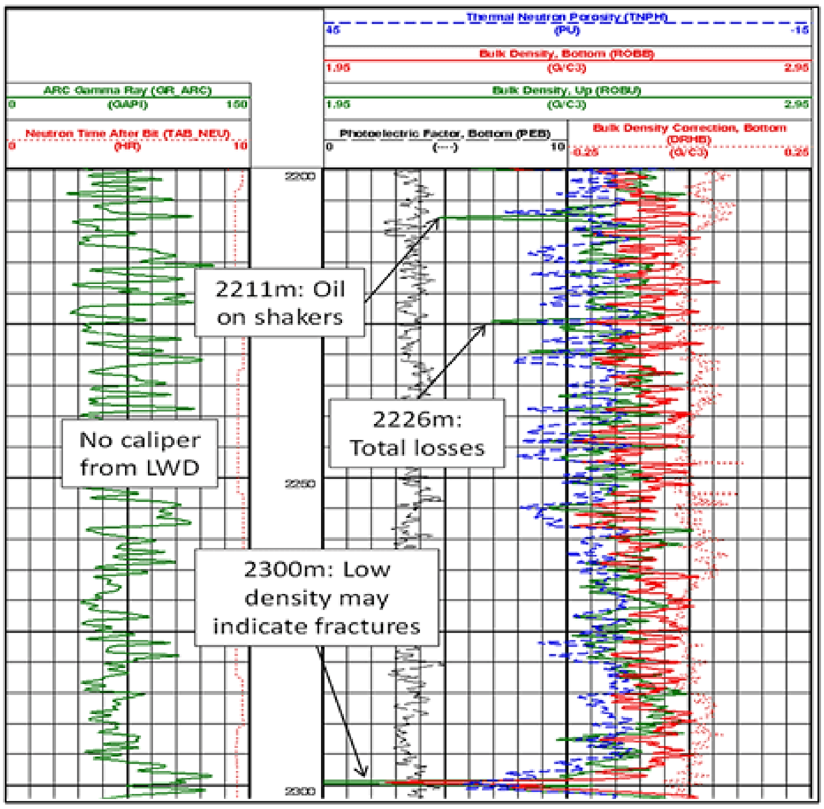

Figure 14. Petrophysics result display in Lam Interval for the Well H-17

The attached data plot illustrates the well performance during the main period. Bottom hole pressures are 3849 psi set at 2.237.2 m MD RKB. The plot below clearly demonstrates that stabilized flow conditions could not be achieved. At the end of the main flow period the WHP (and also the BHP) dropped – during this phase the oil rate decreased and the well was mainly producing gas. This is mainly due to the low permeability of the tested formation (Figure 16).

Comparison between wireline and core data

Logs data (Gamma Ray ,Porosity, Permeability, Density) values were compared with the core data of the H-28 and JAM-1wells. The core analysis (Gamma Ray, Porosity, Permeability, Density) values and the petrophysical log values studied revealed a significant similarity in values determined by the two different methods. The petrophysical log and core analysis values of the reservoirs in both Wells show approximate linear relationship between the two variables (Figure 17).

Analysis of cross plots

Cross-plots show the relationship between values calculated by well-logs and those derived from core analysis data. The gamma ray log values were plotted against the core gamma ray values and this gives a direct relationship between the two data set except for the reservoir in H-28 and JAM-1

Table 7. Petrophysics Summation for the well Nil-1

Well: NIL-1 Lam	Gross (m)	Net Pay m	Vsh (%)	Porosity (%)	SH (%)	Perm mD	HCPV (m)	Fluid
2268 - 2318 m	50	15	57	6/13	33/42	0.2/1.6	0.9	Oil

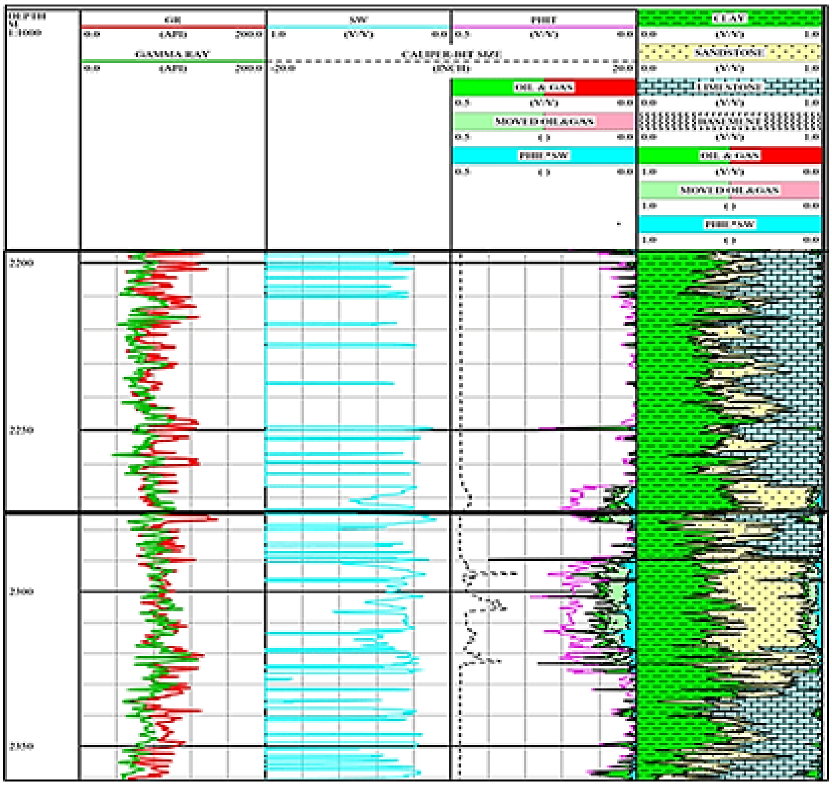

Figure 15. Petrophysical log interpretation of test interval in lower Lam Member of NIL-1 well showing better reservoir quality and movable oil saturation.

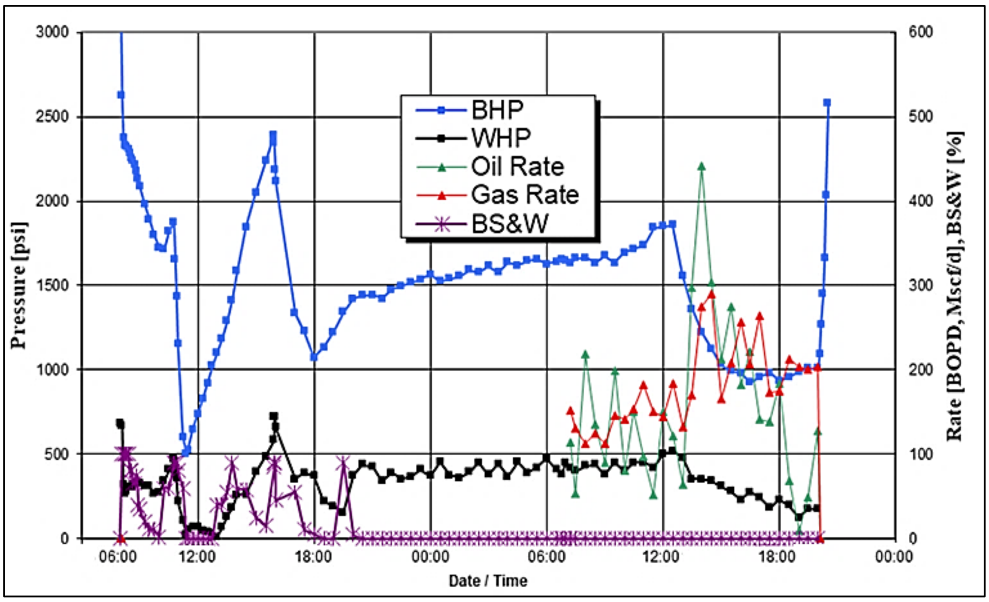

Figure 16. Plot of Pressures & Rates vs Time - Main Flow Period.

wells, which an inverse relationship between the two data was noticed, the inverse relationship is inferred to be as a result of the core gamma ray data which might have loss its physical and chemical properties during analysis in the laboratory (Figure 18).

The density log values were plotted against density core values show that there is a consistent, straight-line relationship between the two, except for the reservoir zones, where both data sets tend to an inverse relationship. Each log shows the volume of shale in its own way.

Through the straight-line region, changes in porosity typically involve changes in shale content. However, in the very clean sandstone, there are variations in porosity that do not involve shale, and the relationship between the two logs changes. The sands in the H-28 well reservoirs are oil-filled, except for a particular Lam reservoir, which is gas-filled (Figure 19).

CONCLUSION

The purpose of the proposed work was to review the applicability of the existing petrophysical evaluations of the Lam Reservoir in the Habban Field. This objective has been addressed, finding that existing log evaluations of the Lam Reservoir are consistent and provide properties similar to those seen in the core and to investigate using the existing conventional logs to determine the properties and hydrocarbon saturation in any laminated reservoir elements. This objective too has been met, with estimates of porosity, permeability and oil saturation in sand laminae being made. This data provides a clearer view of which intervals are likely to flow oil on test.

From the work carried out by the integrated well log petrophysical analysis, subsurface geology, and formation evaluation of Lam Member (Late Jurassic) at the seven wells in Habban oilfield the following conclusions could be outlined:

- The Late Jurassic rocks of the Lam Member are a tight or unconventional reservoir, encountered in the study area from 250 to up to 500 m, that will rely on Perforating, natural fracturing, and/or fracture stimulation to produce. The Lam Member consists of an interbedded sequence of claystone with intercalated sandstone and carbonate (limestone and dolomite) with claystone and intercalated sandstone.
- The shale content in Lam Member increases from the southwestern to the north and northeastern parts of the study area. The abundant shale content in the Lam Member section varies from (15%) to (25%).
- The average porosity of Lam Member rocks in the studied seven wells is generally moderate and ranges from (6%) to (22%).

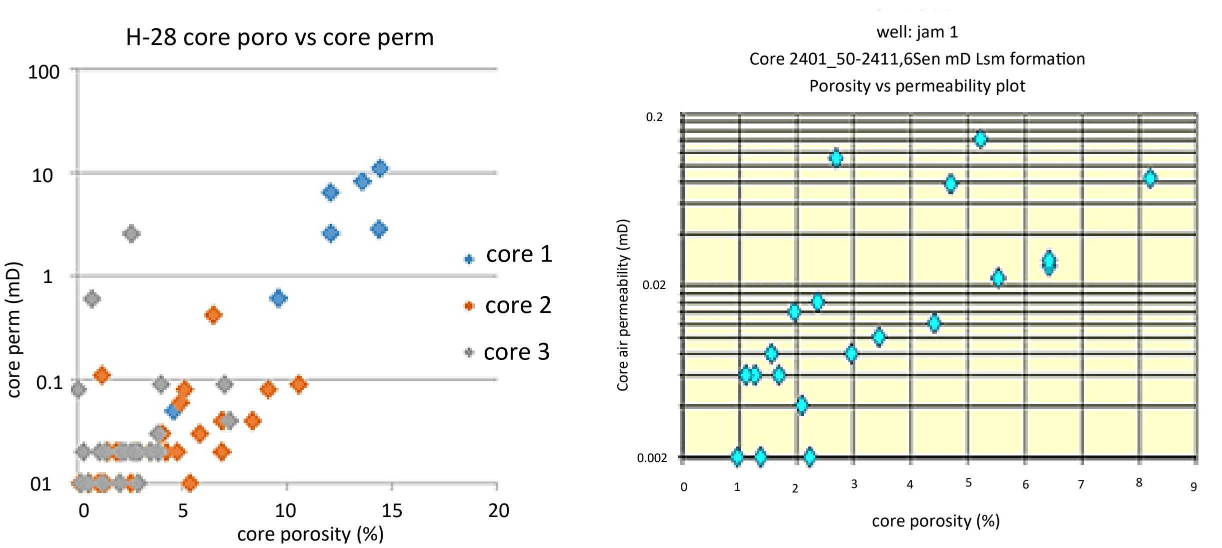

Figure 17. H-28 and JAM-1 wells cross plot (RCA) core permeability (Perm) versus core porosity (Phi).

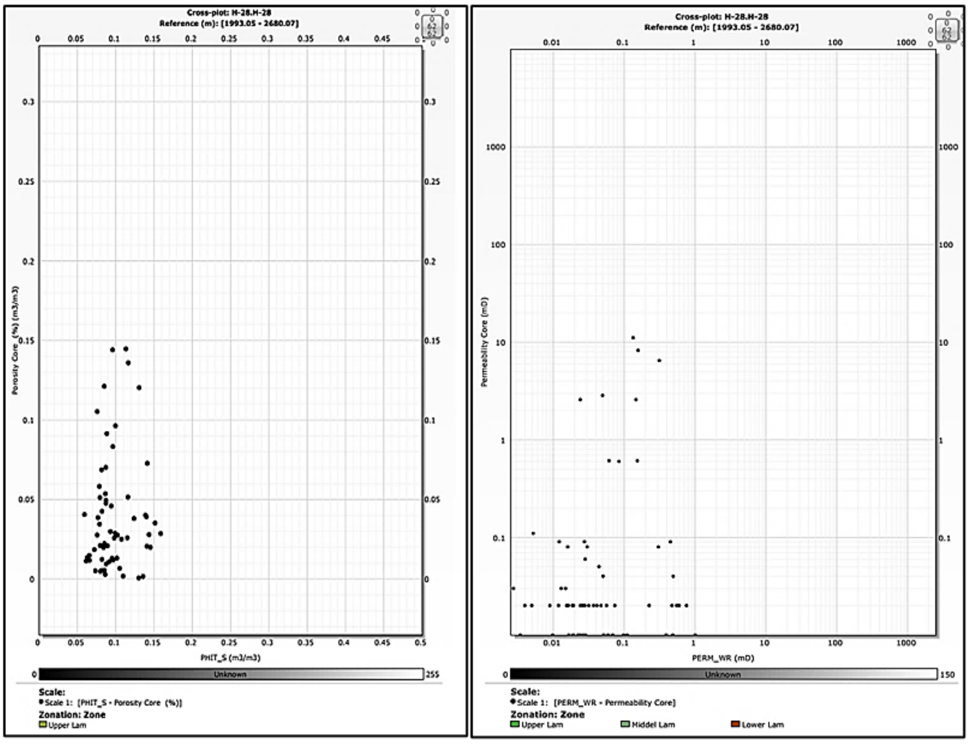

Figure 18. H-28 Cross Plot Core Porosity (Phi) Versus Log Porosity (PHIT) and Cross Plot Core Permeability (Perm) versus Log Permeability.

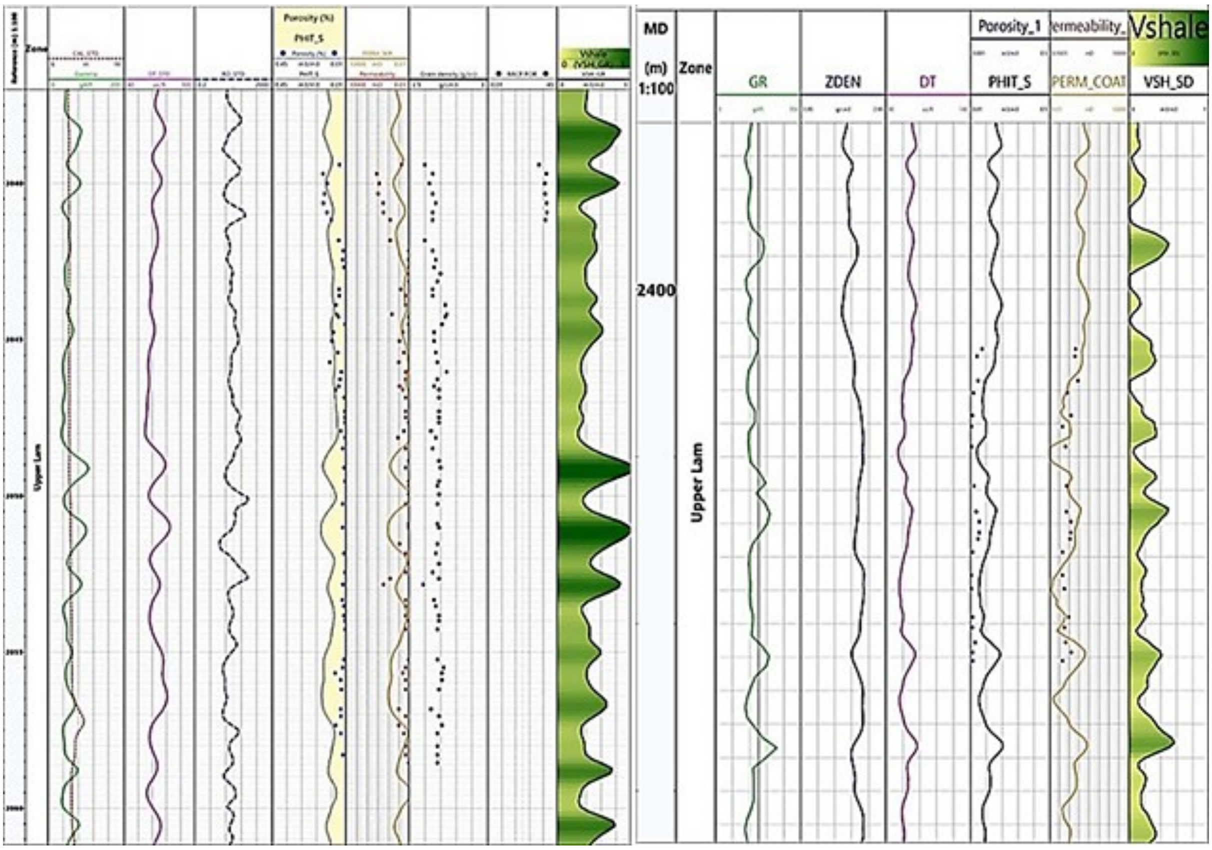

Figure 19. Log and Core Data matching at Lam Reservoir in the wells, Left- H-28 and Right-M-1

- The hydrocarbon saturation of Lam Member increases towards the northeastern parts of the study area recording the highest value of (70 %), whereas it decreases in the middle of the study area recording (15%) towards the northeastern parts These results lead to consider Lam Member as promising for future hydrocarbon exploration in Habban Oil Field.
- The density log-derived porosity compares well with the core data i.e. they give similar ranges. In addition, the results from the two wells are consistent, confirming that this porosity evaluation methodology is appropriate.
- The permeability estimated from the conventional logs (using a core-based porosity to permeability transform) is in close agreement with the core permeability. The formation pressure tester derived permeability is also in reasonable agreement with the log estimates when a viscosity of 0.5 cP is assumed for the fluid combination being flowed.
- From the limited formation pressure data examined, it is possible that different oil columns are present in the Lam Formation, although the configuration looks unusual. The water-bearing or residual oil sections encountered in Habban good lam wells, which appear to be the better porosity (and permeability) units.
- Petrophysical Log interpretation of the test interval in lower Lam member of NIL-1 well showing good reservoir quality and movable oil sat.

ACKNOWLEDGEMENT

The authors would like to express their deepest appreciation to all who support this study. I am also grateful to the Department of Petroleum Engineering at Sana'a University for supporting and providing all requirements".

DECLARATIONS

Author contribution

A. S. Ghurab, A. M. Al-Matary, A. N. Al-Dujaili: Writing – Original Draft, Writing – Review & Editing, Conceptualization, Formal analysis, Investigation, Visualization, Supervision. Al-Khirbash, B. S.: Writing – Review & Editing, Validation, Investigation. Hakimi, M. H.: Writing – Review & Editing, Validation, Investigation. Al-Audi, A. S.: Writing – Review & Editing, Validation, Investigation. All authors read and approved the final paper.

Funding statement

This research did not receive any specific grant from funding agencies in the public, commercial, or not-for-profit sectors.

Competing interest

The authors declare that they have no known competing financial interests or personal relationships that could have appeared to influence the work reported in this paper.

The use of AI or AI-assisted technologies

The authors did not use AI or AI-assisted technologies in the preparation of this work.

GLOSSARY OF TERMS AND SYMBOLS

Terms & Symbols	Definition	Unit
a	Tortuosity factor (Archie's constant)	-
A28H	Phase Shift Resistivity at 28 inches spacing, 2 mhz, corrected	ohm·m
A40H	Component log for a Heat & Glo fireplace	-
Avg.	Average	-
b/e	Barns per electron	-
BHI	Borehole image log	-
CAL	Caliper	Inch
CNC	Compensated neutron log	Fraction
DAL	Data access layer	M
DLL	Deep lateral log	
DT	Sonic log	µs/ft
GR	Gamma ray	API
H	Habban field	-
Jam	Al-Jameelah well	-
K	Permeability	mD.
LCM	Lost circulation material	-

LWD	Logging while drilling tool	-
m	Cementation exponent	-
n	Saturation exponent	-
NIL	Al Nilam well	-
NPHI	Neutron porosity	Fraction
ϕ	Porosity	%
P16H	Resistivity log used while drilling	ohm·m
P28H	Phase Shift Resistivity at 28 inches spacing, 2 mhz, corrected	ohm·m
P40H	Deep-sensing phase resistivity	ohm·m
PE	Photoelectric index	-
PEB	Process environment block	-
PEF	Photoelectric Factor log	b/e
PEPA	Petroleum Exploration and Production Authority-Yemen	-
Perm	Permeability	mD.
PHIT	Total porosity	Fraction
RCA	Routine core analysis	-
RD	Deep resistivity	ohm·m
Res	Reservoir	-
RKB	Rotary kelly bushing	-
RMLL	Medium resistivity lateral log	ohm·m
ROHB	Density log	gm/cm^3
RS	Shallow resistivity	ohm·m
Sh	Hydrocarbon saturation	%
SP	Spontaneous potential	mV
Sw	Water saturation	%
TNPH	Thermal neutron porosity	%
TTRM	Transformer turns ratio meter	V
TVT	True vertical depth	M
Vsh	Shale volume	%
XRD	X-ray Diffraction	-
ZDEN	Density log	gm/cm^3
ZDL	Litho-density log	gm/cm^3

REFERENCES

Abilkhasimov, K. B., Jangirov, A. N., Al-Dujaili, A. N., Nunoo, S., & Tileuberdi, N. (2025). Sedimentation Stages of the Temir Carbonate Platform Formation in the Caspian Sedimentary Basin during the Late Paleozoic. ES Energy and Environment, 29, 1706. http://dx.doi.org/10.30919/ee170

Abudeif, A. M., Radwan, A. E., Al-Azazi, N. A., Mohammed, M. A., & Basrada, F. M., (2024). Petrophysical Parameters and Reservoir Evaluation from Well Log Analysis of Lam Member (Late Jurassic), Habban Oil Field, Marib-Shabwah (Sab'atayn) Basin, Yemen. Sohag Journal of Sciences, 9(1), 86-93. https://doi.org/10.21608/sjsci.2023.224819.110

Adams, S., (2011). Habban Lam Petrophysical Update internal report for OMV Yemen Block S2. Well, Eval.com Pte. Ltd.WCL110906. Singapore.

Ahlbrandt, T.S., (2002). Madbi Amran/Qishn Total Petroleum System of the Marib–Al Jawf/ Shabwah, and Masila-Jeza Basins, Yemen. United States Geological Survey Bulletin, 2202-G, 28 p.

Al-Areeq. Nabil, M. and, Albaroot. Mohammed. A., (2019). Source rocks evaluation and thermal maturity evolution of the Dhamar Ali field, Sab'atayn basin, Yemen, Asian Journal of Science and Technology, 10(01), 9364-9374.

Al-Areeq. Nabil. M., & Albaroot. Mohammed. A., (2018) .Petroleum source rocks characterization and hydrocarbon generation of the Upper Jurassic succession in Jabal Ayban field, Sabatayn Basin, Yemen. Egyptian Journal of Petroleum, 27(4), 835 -851. https://doi.org/10.1016/j.ejpe.2017.12.00

Albaroot, M., Elhossainy, M. M., Al-Areeq, N. M., Abdullah, E. A., & Salman, A. M., (2024). The Upper Jurassic sediments, Marib-Shabwa Basin, Yemen: lithofacies aspects and sequence stratigraphic analysis. Energy Geoscience, 5(1), 100214. https://doi.org/10.1016/j.engeos.2023.10021

Albaroot. M, Ahmad. A. H. M, Al-Areeq. Nabil, Sultan. M., (2016). Tectonostratigraphic of Yemen and Geological Evolution: A New Prospective. International Journal of New Technology and Research (IJNTR) ISSN:2454-4116, Volume-2, Issue-2, Pages 19-33.

Al-Dujaili, A. N., (2023). Reservoir rock typing and storage capacity of Mishrif Carbonate Formation in West Qurna/1 Oil Field, Iraq. Carbonates and Evaporites, 38(4). https://doi.org/10.1007/s13146-023-00908-

Al-Dujaili, A. N., (2024). Reservoir and rock characterization for Mishrif Formation/ Zubair Field

(Rafdiya and Safwan Domes) by nuclear magnetic resonance and cores analysis. Iraqi Journal of Chemical and Petroleum Engineering, 25(3), 1–14. https://doi.org/10.31699/ijcpe.2024.3.

Al-Matary, A. M., (2007). Geo-history, Microfacies and Petroleum Assessment of the Central Part of the Sab'atayn Basin, Yemen. PhD thesis. Yarmouk University of Jordan, Jordan.

Al-Matary. A. M, Hakimi. M. H, Al Sofi. S, Al-Nehmi. Y. A, Al-haj. M. A, Al-Hamdani. A, Al-Sarhi. A., (2018). Preliminary source rock evaluation and hydrocarbon generation potential of the early Cretaceous subsurface shale from Shabwah subbasin in the Sabatayn Basin, Western Yemen. Journal of African Earth Science, 142. https://doi.org/10.1016/j.jafrearsci.2018.02.00

Al-Matary. A. M., (2003). Petrography and Hydrocarbon Potentiality Studies of the Middle-Upper Jurassic Amran Sediments (Amran Group) in Sab'atayn Basin, Yemen. M.Sc. thesis. Yarmouk University, Jordan.

Al-Wosabi, M., Saeed O. Wasel, (2011) Lithostratigraphic subdivision of the Kuhlan Formation in Yemen, Arabian Journal of Geosciences. https://doi.org/10.1007/s12517-010-0236-

As-Saruri, M. A., R. Sorkhabi, and R. Baraba., (2010). Sedimentary basins of Yemen: Their tectonic development and lithostratigraphic cover. Arabian Journal of Geosciences, 3(4):515–27. https://doi.org/10.1007/s12517-010-0189-

Bawazer, W., Lashin, A., & Kinawy, M. M. (2018). Characterization of a fractured basement reservoir using high-resolution 3D seismic and logging datasets: A case study of the Sab'atayn Basin, Yemen. PLoS One, 13(10), e0206079. https://doi.org/10.1371/journal.pone.020607

Beydoun, Z.R., (1991). Arabian Plate Hydrocarbon Geology and Potential - A Plate Tectonic Approach. American Association of Petroleum Geologists Studies in Geology No. 33, 77 p. https://doi.org/10.1306/St3353

Beydoun, Z.R., As-Saruri, M.A.L., El-Nakhal, H., Al-Ganad, I.N., Baraba, R.S., Nani, A.S.O. and Al-Aawah, M.H., (1998). International lexicon of stratigraphy, Volume III, Republic of Yemen, 2nd ed.: International Union of Geological Sciences and Ministry of Oil and Mineral Resources, Republic of Yemen Publication 34, 245 p.

Beydoun, Z.R., As-Saruri, M.L. and Baraba', R.S., (1996). Sedimentary basins of the Republic of Yemen: Their structural evolution and Geological characteristics. Revue de l' Institute Francia's du Petrol, 51: 763-775. https://doi.org/10.2516/ogst:199604

Bosence, D.W.J., (1997). Mesozoic rift basins of Yemen. Marine and Petroleum Geology, 14: 611-616. https://doi.org/10.1016/S0264-8172(97)00039-

Brannin. J, Sahota. Gurdip, Gerdes. KD, Berry. JAL., (1999). Geological evolution of the central Marib-Shabwah basin, Yemen. Geo Arabia; 4:9–34. https://doi.org/10.2113/geoarabia04010

Casto, I., A. Habib, K. Kiss, I. Kocz, Z. Kovacs, K. Lorincz, and K. Milota, (2001). Play concepts of oil exploration in Yemen: Oil and Gas Journal, 99, 68–74.

Edgell, H. S. (2006). Arabian deserts: nature, origin, and evolution. Dordrecht: Springer Netherlands. https://doi.org/10.1007/1-4020-3970-

El-Ata, A. S. A., EI-Khafeef, A. A., Ghoneimi, A. E., Abd Alnabi, S. H., & Al-Badani, M. A., (2013). Applications of aeromagnetic data to detect the Basement Tectonics of Eastern Yemen region. Egyptian Journal of Petroleum, 22(2), 277-292. https://doi.org/10.1016/j.ejpe.2013.06.00

Elhossainy, M. M., Albaroot, M., Al-Areeq, N. M., & Salman, A. M., (2022). Late Jurassic Safir evaporite salts, Sab'atayn Basin, Yemen: Lithofacies distribution, cyclicity, and mineralogy. Journal of African Earth Sciences, 195, 104641. https://doi.org/10.1016/j.jafrearsci.2022.10464

Ellis, A.C., Kerr, H.M., Cornwell, C.P., Williams, D.O., (1996). A tectonostratigraphic framework for Yemen and its implications for hydrocarbon potential. Petroleum Geoscience, no. 2, p. 29-

42. https://doi.org/10.1144/petgeo.2.1.2

Ghiglione, G., & Abbasi, I., (2012, November). Tectonic discontinuities analysis using seismic and well datasets in a fractured basement reservoir. In Abu Dhabi International Petroleum Exhibition and Conference (pp. SPE-162399). SPE. https://doi.org/10.2118/162399-M

Hadden, R. L., (2012). The geology of Yemen: An annotated bibliography of Yemen's geology, geography and earth science.

Hakimi, M. H., Al-Matary. A. M. and, Salad Hersi. O., (2018) ‘Late Jurassic bituminous shale from Marib oilfields in the Sabatayn Basin (NW Yemen). Geochemical and petrological analyses reveal oil-shale resources. The science and technology of Fuel and Energy, Fuel, 232 530–542. https://doi.org/10.1016/j.fuel.2018.05.13

Hakimi, M. H., Varfolomeev, M., Qadri, S. M. T., Lashin, A., Yelwa, N. A., Radwan, A., & Saeed, S., (2022). Overview of the Late Jurassic Madbi -Sab'atayn petroleum system in the Marib Concession, northwestern Sab'atayn Basin (Yemen): hydrocarbon from source to trapping. Arabian Journal of Geosciences, 15 (3), 319. https://doi.org/10.1007/s12517-022-09576-

Hatem, B. A., Abdullah, W. H., Hakimi, M. H., & Mustapha, K. A., (2016). Origin of organic matter and paleoenvironment conditions of the Late Jurassic organic-rich shales from Shabwah sub-basin (western Yemen): Constraints from petrology and biological markers. Marine and Petroleum Geology, 72, 83-97. https://doi.org/10.1016/j.marpetgeo.2016.01.01

Khashman, M. A., Shirazi, H., Al-Dujaili, A. N., & Sulaiman, N. M., (2025). Maximizing oil recovery and economic returns through strategic well spacing in the Mishrif Formation, Southern Iraq. Modeling Earth Systems and Environment, 11(6). https://doi.org/10.1007/s40808-025-02609-

Mabon, S., & Mason, R., (2022). Gulf States and the Horn of Africa: Interests, influences and instability. https://doi.org/10.7765/978152616217

Oktaviany, A. P., DN, A. A. P., Farahdibah, U., Maharsi, D. A., Astuti, W., & Gibrata, M. A. (2022). Digital Core Analysis of Capillary Pressure in Sandstone. *Scientific Contributions Oil and Gas*, 45(3), 183-191. https://doi.org/10.29017/SCOG.45.3.126.

Ragil, D., Muthofa, M. A., Wahyudi, W., Mutakim, M. A., Oktiviannysa, E., Aji, N. T., & Prakoso, Y. H. (2024). Perancangan Alat Desorpsi Gas pada Sampel Batuan Serpih Guna Pengukuran Volume Gas pada Skala Laboratorium. *Lembaran Publikasi Minyak dan Gas Bumi (LPMGB)*, 58(2), 103-113. https://doi.org/10.29017/LPMGB.58.2.164

Redfern, P., Jones, J.A., (1995). The interior rift of The Yemen-analysis of basin structure and stratigraphy in a regional plate tectonic context. Basin Research, No. 7, 337-356. https://doi.org/10.1111/j.1365-2117.1995.tb00121.

Ronlei, B. C., Wibowo, A. S., Sigalingging, A. S., Nathania, E. Y., Fatkhan, F., Erdi, A., ... & Husein, A. A. A. (2025). Reservoir Characterization of Ngrayong Formation, Sandstone with Carbonate Intercalation, Using a Geostatistical Approach Based on Petrophysical Parameters, Northeast Java Basin, Indonesia. *Scientific Contributions Oil and Gas,* 48(3), 237-251. https://doi.org/10.29017/scog.v48i3.182.

Sachsenhofer, R. F., Bechtel, A., Dellmour, R. W., Mobarakabad, A. F., Gratzer, R., & Salman, A., (2012). Upper Jurassic source rocks in the Sab’atayn Basin, Yemen: Depositional environment, source potential and hydrocarbon generation. GeoArabia, 17(4), 161-186. https://doi.org/10.2113/geoarabia170416

Seaborne, T. R., (1996). The influence of the Sabatayn Evaporites on the hydrocarbon prospectivity of the Eastern Shabwa Basin, Onshore Yemen. Marine and Petroleum Geology, 13(8), 963-972. https://doi.org/10.1016/S0264-8172(96)00017-

Sellar. C, Zabalza. I, and, Miguel. K., (2014). Less is More: An Objective/Cost-Driven Approach to Reducing Uncertainty in the Appraisal of the Lam Reservoir, Central Yemen. Society of Petroleum Engineers. Paper presented at the Abu Dhabi

International Petroleum Exhibition and Conference, Abu Dhabi, UAE. Paper Number: SPE-171875-MS. https://doi.org/10.2118/171875-M

Stephenson, M. H., & Kader Al-Mashaikie, S. A. Z. A., (2011). Stratigraphic note: update on the palynology of the Akbarah and Kuhlan formations, northwest Yemen. GeoArabia, 16(4), 17-24. https://doi.org/10.2113/geoarabia16041

Uzbekgaliev, R., Al-Dujaili, A. N., Tileuberdi, N., Auelkhan, E., Togizov, K., Amralinova, B., Akbarov, E., & Sanatbekov, M., (2025). Lithological Types of Deposit - a new strategy for exploration works for oil and gas in southern Mangushlak, Kazakhstan. ES Energy & Environments, 29, 1681. https://doi.org/10.30919/ee168

Wardhana, R., Yasutra, A., Irawan, D., & Haidar, M. W. (2022). A Case Study of Primary and Secondary Porosity Effect for Permeability Value in Carbonate Reservoir using Differential Effective Medium and Adaptive Neuro-Fuzzy Inference System Method. *Scientific Contributions Oil and Gas*, 45(1), 13-22. https://doi.org/10.29017/SCOG.45.1.92.

Watchorn, F., Nichols, G. J., & Bosence, D. W. J., (1998). Rift-related sedimentation and stratigraphy, southern Yemen (Gulf of Aden). In Sedimentation and Tectonics in Rift Basins Red Sea:-Gulf of Aden (pp. 165-189). Dordrecht: Springer Netherlands. https://doi.org/10.1007/978-94-011-4930-3_1.

Worden, R. H., (2006). Dawsonite cement in the Triassic Lam Formation, Shabwa Basin, Yemen: A natural analogue for a potential mineral product of subsurface CO2 storage for greenhouse gas reduction. Marine and Petroleum Geology, 23(1), 61-77. https://doi.org/10.1016/j.marpetgeo.2005.07.00

Ziegler, M.A., (2001). Late Permian to Holocene Paleo facies Evolution of the Arabian Plate and Its Hydrocarbon Occurrences. GeoArabia, 6, 445-504. https://doi.org/10.2113/geoarabia060344